

Adapting LLaMA Decoder to Vision Transformer

Jiahao Wang¹, Wenqi Shao^{2*}, Mengzhao Chen², Chengyue Wu¹, Yong Liu³,
Kaipeng Zhang², Songyang Zhang², Kai Chen², Ping Luo^{1*}

¹The University of HongKong. ²Shanghai AI Laboratory.

³Tsinghua Shenzhen International Graduate School.

jiahao.wang@connect.hku.hk, shaowenqi@pjlab.org.cn

Abstract

This work examines whether decoder-only Transformers such as LLaMA, which were originally designed for large language models (LLMs), can be adapted to the computer vision field. We first “LLaMAfy” a standard ViT step-by-step to align with LLaMA’s architecture, and find that directly applying a causal mask to the self-attention brings an attention collapse issue, resulting in the failure to the network training. We suggest to reposition the class token behind the image tokens with a *post-sequence class token* technique to overcome this challenge, enabling causal self-attention to efficiently capture the entire image’s information. Additionally, we develop a *soft mask* strategy that gradually introduces a causal mask to the self-attention at the onset of training to facilitate the optimization behavior. The tailored model, dubbed as *image LLaMA (iLLaMA)*, is akin to LLaMA in architecture and enables direct supervised learning. Its causal self-attention boosts computational efficiency and learns complex representation by elevating attention map ranks. iLLaMA rivals the performance with its encoder-only counterparts, achieving 75.1% ImageNet top-1 accuracy with only 5.7M parameters. Scaling the model to ~310M and pre-training on ImageNet-21K further enhances the accuracy to 86.0%. Extensive experiments demonstrate iLLaMA’s reliable properties: calibration, shape-texture bias, quantization compatibility, ADE20K segmentation and CIFAR transfer learning. We hope our study can kindle fresh views to visual model design in the wave of LLMs. Pre-trained models and codes are available here.

1 Introduction

The year 2024 saw the meteoric rise of large language models (LLMs), as well as the 4th anniversary of the Vision Transformer (ViT) [14]. Born in 2020, ViT has revolutionized the computer vision field by adapting the Transformer [58], which was originally designed for natural language, to process images as non-overlapping patches. Notably, ViT design was influenced by the prevailing *encoder-only* text Transformers at the time, such as BERT [12], *etc.* Accordingly, ViT is allowed to borrow the encoder-only design, *i.e.*, self-attention do not use any causal mask. As a result, advanced vision backbones [51, 61, 23] and training paradigms [3, 25] have followed such convention by default.

Meanwhile, the development of text Transformers did not stand still. A series of LLMs with a *decoder-only* architecture, such as LLaMA [53, 54], OPT [70], and PaLM [8], have sparked a new wave. Pre-trained decoder-only Transformers have demonstrated remarkable scalability with respect to model capacity and training data in diverse textual tasks. This revolution naturally raises a new issue, *i.e.*, the misalignment between encoder-only visual and decoder-only textual architecture.

In the era of LLMs, could decoder-only Transformers be revitalized in the vision field? In this study, we demonstrate that through straightforward supervised learning, LLaMA architecture itself

*Corresponding author.

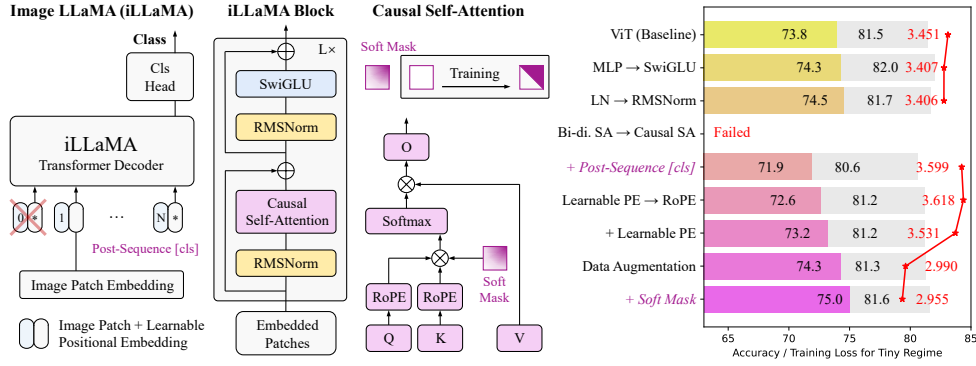


Figure 1: Left: iLLaMA architecture. Right: the design roadmap. Colored and gray bars represent the results of the tiny and base regimes, with the red line depicting the training loss of the tiny regime. iLLaMA strives to process visual tokens using standard LLaMa components, e.g., causal self-attention. The proposed *PS [cls]* and *soft mask* strategy help overcome training challenges. Block details of ViT [14], VisionLLaMA [9], and our iLLaMA is compared in Figure 5 in Appendix A.

can process input images with simple yet crucial modifications. We start by modifying a standard encoder-only ViT (e.g., ViT-T/16), progressively adapting its components to align with those in LLaMA. In practice, we observe an *attention collapse* issue, i.e., the training loss fails to converge by directly adding a causal mask to the attention map. The causal mask restricts the class token from accessing the image’s global information, thereby hindering the optimization of the training loss. To this end, we propose a *post-sequence class token* technique, repositioning the class token to the end of image tokens (details in Section 3.3). As a result, causal mask can keep the attention score between the class token and others, allowing the model to optimize stably. We also evaluate the advantages of the causal self-attention in reducing computational complexity and enhancing the attention map rank.

Moreover, we explore several training techniques for the proposed causal Transformer. When observing things, humans start by broadly catching global connections, then narrow down to focus on specifics. Motivated by this, we develop a *soft mask* approach – bi-directional self-attention degenerates to a causal self-attention at the onset of training – to further boost the network performance. Soft mask does not alter the causal self-attention during inference but improves the initial training behavior of the network. (details in Section 3.6). We illustrate different types of masks in Figure 3.

Equipped with such modifications, we propose a non-autoregressive decoder-only vision Transformer with causal self-attention inside, dubbed *image LLaMA (iLLaMA)*, as shown in Figure 1. We provide a block level comparison of ViT [14], VisionLLaMA [9], and our iLLaMA in Figure 5 in Appendix A. iLLaMA process visual input with our slightly modified causal self-attention. We conduct a comprehensive evaluation of iLLaMA’s properties, including ImageNet-1K classification [11], calibration, shape-texture bias, quantization compatibility, ADE20K semantic segmentation [72], and CIFAR transfer learning [31]. Experimental results show that iLLaMA delivers favorable and reliable performance to its encoder-only counterparts (i.e., ViT, VisionLLaMA), while maintaining a pure decoder design. More importantly, a spectral analysis on the attention map empirically shows that compared to bi-directional counterparts, causal self-attention has a higher rank (see Figure 4), which allows for learning complex image representation. We hope our work to inspire a re-evaluation of vision backbone design in the era of LLMs and provide fresh insights for their architectural unification.

2 Preliminaries and Motivation

Encoder and decoder. We briefly summarize the encoder and decoder in Transformer [58]. Both of them basically consist of attention module and a MLP module, each followed by a residual connection. *The key difference between them is the mask scheme in their self-attention.* Encoders use bi-directional self-attention, and decoders employ causal self-attention and cross-attention. However, the latter is typically omitted in decoder-only LLMs [53, 54], we thus focus on comparing causal and bi-directional self-attention as follows, in terms of the *mask* setting. Denote $\mathbf{X} \in \mathbb{R}^{N \times d}$, $\mathbf{O} \in \mathbb{R}^{N \times d}$ as the input and output sequences, where N is the number of tokens and d is the embedding dimension. $W_q, W_k, W_v \in \mathbb{R}^{d \times d}$ denotes the linear mapping of query, key and value, respectively. Generally, self-attention module can be formulated as (set the head number and batch size as 1 for simplicity):

$$\mathbf{A} = \frac{1}{\sqrt{d}}(W_q(\mathbf{X}) \cdot W_k(\mathbf{X})^\top), \quad \mathbf{O} = \text{Softmax}(\mathbf{A} + \mathbf{M}) \cdot W_v(\mathbf{X}), \quad \mathbf{P}_{i,j} = 0, \quad \mathbf{Q}_{i,j} = \begin{cases} 0, & i \geq j \\ -\infty, & i < j \end{cases} \quad (1)$$

where $i, j \in [1, N]$, $\mathbf{A} \in \mathbb{R}^{N \times N}$, $\mathbf{M} \in \mathbb{R}^{N \times N}$ denote the attention map and mask. $\mathbf{P} \in \mathbb{R}^{N \times N}$, $\mathbf{Q} \in \mathbb{R}^{N \times N}$ are masks in the encoder and decoder, respectively. For a causal self-attention, we have $\mathbf{M} = \mathbf{Q}$. Such design allows subsequent tokens only attend to the preceding ones, but not vice versa. For a bi-directional self-attention, we have $\mathbf{M} = \mathbf{P}$, ensuring mutual visibility for each token.

Autoregressive (AT) and non-autoregressive (NAT) models. AT models have demonstrated remarkable generation ability in LLMs [53, 54]. Besides the text domain, AT models have also been widely used in image [57, 56, 46, 42, 6] and audio [38] tasks. Unlike the stepwise computation paradigm of the AT models, NAT models [73, 45, 4, 20, 21] generate all output tokens in parallel, thereby controlling the output length easily and reducing inference latency. Our iLLaMA allows for one-step inference and consists entirely of NAT decoders, making it suited for visual perception tasks.

Recent LLMs-related image models. Recent image models [2, 24, 15] are trained with an autoregressive objective, targeting at solving visual tasks. Pang et al. [39] add a text pre-trained frozen LLM block to a ViT encoder to facilitate the performance. Our work, on the other hand, is motivated to explore in-depth how the decoder design in LLMs can be adapted to image models using simple supervised learning to achieve an architectural alignment. A concurrent work VisionLLaMA [9] proposes vision models for recognition and generation tasks based on the LLaMA components. Differently, we: 1) introduce causal self-attention from LLaMA, addressing the associated attention collapse issue, while VisionLLaMA retains an encoder architecture; 2) develop a soft mask technique to assist training the decoder; 3) expand the dataset to the larger ImageNet-21K to demonstrate scalability, achieving 86.0% ImageNet accuracy that outperforms VisionLLaMA’s best results.

3 A Roadmap: Solving Attention Collapse and Optimization Improvement

This section introduces the design roadmap of iLLaMA. As we aim to adapt LLMs to vision, we choose LLaMA [53] and ViT [14] as language and vision references in light of their successful practices. The trajectory can be divided into two dimensions, *i.e.*, architecture (Section 3.1-3.4) and training techniques (Section 3.5-3.6). First, we focus on block designs including 1) feed forward network, 2) normalization layer, 3) self-attention, 4) positional embedding, illustrated in Figure 1. Next, we study training techniques and develop a soft mask strategy to facilitate optimization. Finally, we provide an analysis in terms of efficiency and attention map rank (Section 3.7). We start with ViT-T/16 and ViT-B/16 with around 5.7M and 86.4M parameters, respectively, and gradually replace the corresponding components with those from LLaMA. We conduct experiments on ImageNet-1K [11], following the training recipe adopted from [36] (details in Appendix B.1). Considering the differences between visual perception and text generation tasks, we maintain ViT’s non-autoregressive manner in our network. Each step change and the corresponding results are reported in Appendix C.

3.1 Feed Forward Network (FFN)

FFN structure in Transformer are implemented differently in ViT and LLaMa, *i.e.*, multi-layer perceptron (MLP) and SwiGLU [47]. MLP consists of two sequential linear mappings, with a GELU [27] function inserted. Meanwhile, SwiGLU combines three linear mappings, integrating a SiLU [27, 16, 41] function. This structure allows for the modulation of high-dimensional features through a gating mechanism before reduction. We substituted the Transformer’s MLPs with SwiGLUs, while maintaining comparable computational load. As illustrated in Figure 1, this improves performance from 73.8% to 74.3%, and from 81.3% to 82.0% for the ViT-T/16 and ViT-B/16 regime. This improvement highlights SwiGLU’s effectiveness not only in language models but also in vision, inspiring further exploration of other components.

We will now use SwiGLU to substitute MLP in each block.

3.2 Normalization Layer

Transformers need normalization layer for stable training, *i.e.*, layer normalization (LN) [1] in ViT and root mean square layer normalization (RMSNorm) [68] in LLaMA, respectively. We replaced all LNs with RMSNorms in our network and empirically observed that the accuracy of the ViT-T/16 regime increased from 74.3% to 74.5%. However, similar improvements in precision were not observed in the ViT-B/16 regime (from 82.0% to 81.7%). Nonetheless, compared to LN, RMSNorm removes the shift term computation, bringing simplicity to the network [54, 7, 44, 30].

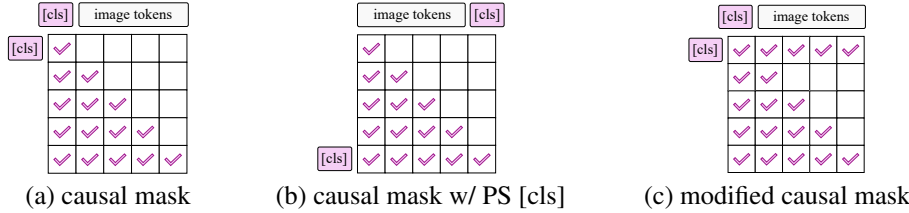


Figure 2: Illustration of different masks in self-attention. From left to right: mask in causal self-attention, mask in causal self-attention with the PS [cls] method, and a modified causal mask.

We will use *RMSNorm* instead of *LN* as the normalization layer in each block.

3.3 causal Self-Attention Leads to Attention Collapse

Attention collapse issue. As a common practice for Transformer decoders, the key component for causal self-attention is the causal mask, *i.e.*, a lower triangular mask matrix, illustrated in Eq. 1 and Figure 2(a). With such, each token can get the attention score of all its previous ones. We add the causal mask to our network via a non-autoregressive way. The reason is that visual perception tasks, unlike text generation, require only inference once. As a result, we observe that the training loss fails to converge in both ViT-T/16 and ViT-B/16 regimes (line 1 in Table 1). We posit that such issue stems from the influence of the lower triangular matrix, which prevents the class token from “seeing” other image tokens. As illustrated in Figure 2(a), when the class token is positioned at the start of the patch embedding, its attention score for all other image tokens gets zero due to a causal mask. We term this occurrence as the *attention collapse* issue, which leads to a loss of connection between the class token and other image patches, thereby hindering the optimization of the network.

Post-sequence class token (PS [cls]). The attention collapse issue stems from the inappropriate placement of the token. To this end, we suggest a *PS [cls]* strategy, by placing it at the end of the token sequence, without changing the causal mask, as shown in Figure 2(b) and Figure 1. Such modification ensures that the class token can achieve global information about all image

Table 1: Results of *PS [cls]* and the modified causal mask. Training converges in both settings.

Model	Tiny	Train Loss	Base	Train Loss
None	0.1	Failed	0.1	Failed
PS [cls]	71.9	3.599	80.6	2.869
Modified	72.5	3.550	80.4	2.857

tokens, while maintaining a causal self-attention property. As a result, we observe that the attention collapse issue is eliminated and the training process starts to stabilize, leading the network performance to 71.9% for ViT-T/16 and 80.6% for ViT-B/16 regime, respectively (line 2 in Table 1).

To test our hypothesis about the reason of the attention collapse issue, we also explore a mask setting in Figure 2(c). In this setting, we do not change the position of the class token. Instead, we unmask the first row of the mask (*i.e.*, attention score of the class token) on the basis of the causal self-attention, termed as “modified causal mask”. Ablation results (line 3 in Table 1) shows that both settings can solve the attention collapse issue as expected, and the “modified causal mask” leads to a better 72.5% accuracy for ViT-T/16 regime, validating our hypothesis about the reason. Although the results do not surpass the performance of bi-directional counterpart, they demonstrate the potential for optimizing causal self-attention in a decoder-only image model. We also observe that the *PS [cls]* method yields higher accuracy with a slightly larger training loss for ViT-B/16 regime, suggesting lower overfitting.

We will employ causal self-attention with *the proposed PS [cls] method* in each block.

3.4 Positional Embedding

A standard ViT use learnable positional embedding (LPE) to preserve positional information, typically adding it directly to the patch embedding. Meanwhile, rotary positional embedding (RoPE) [49] is widely employed in LLMs [53, 54], which functions within the attention of each block. We first use RoPE alone, which boosts the accuracy of ViT-T/16 and ViT-B/16 regimes to 72.6% and 81.2%, respectively. The encouraging results illustrate that the concepts of “position” in image and text do not exist an inherent gap. Since LPE functions only once before all Transformer blocks, keeping it does not disrupt the alignment with LLaMA within each block. Thus, we reintroduce the LPE, which improves the accuracy of ViT-T/16 regime to 73.2%, suggesting that the two positional embeddings are not redundant but rather synergistic, contributing to the network performance.

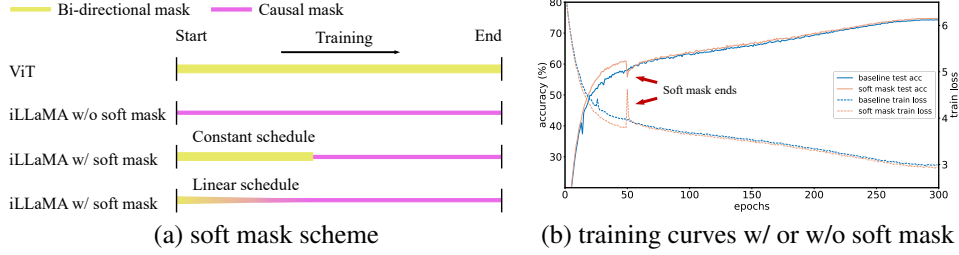


Figure 3: Left: soft mask gradually transitions from a bi-directional mask into a causal mask during training through a constant or linear schedule. Right: ablation training loss and test accuracy.

We will use both *LPE* and *RoPE* for positional embedding. So far, we have investigated each block component, and thus fix the final architecture dubbed iLLaMA. Next, we explore training strategies.

3.5 Data Augmentation

Mixup [69] and cutmix [67] that we used to train our iLLaMA (0.8 and 1.0), are borrowed from DeiT [51]’s recipe. Unlike the bi-directional self-attention used in DeiT, causal self-attention affects the connection between image tokens. Meanwhile, these two hyper-parameters affect the content of the input image, which further influences the subsequent embedding. Thus, we reevaluate their impact on iLLaMA optimization. Specifically, we discover that a combination of 0.1 mixup and 0.1 cutmix improves the performance of the iLLaMA-T/16 to 74.3%, whereas a combination of 0.95 and 1.0 leads the iLLaMA-B/16 to a 81.3% accuracy. Other ablations are detailed in Section 4.1.

3.6 Soft Mask Strategy: Optimization Improvement

When observing objects, humans tend to perceive broad connections, then focus on specific details. Motivated by this, we propose a *soft mask* technique to improve the model’s optimization: *starting with bi-directional self-attentions in the early training epochs and gradually shifting completely to causal self-attentions as the optimization goes*. Specifically, self-attention can be formulated as:

$$\mathbf{A} = \frac{1}{\sqrt{d}}(W_q(\mathbf{X}) \cdot W_k(\mathbf{X})^\top), \quad \mathbf{O} = (\text{Softmax}(\mathbf{A}) \odot \mathbf{S}) \cdot W_v(\mathbf{X}), \quad (2)$$

$$\mathbf{S} = \alpha \mathbf{B} + (1 - \alpha) \mathbf{C}, \quad \mathbf{B}_{i,j} = 1, \quad \mathbf{C}_{i,j} = \begin{cases} 1, & i \geq j \\ 0, & i < j \end{cases}$$

where $i, j \in [1, N]$, $\mathbf{S} \in \mathbb{R}^{N \times N}$ denotes the soft mask, which is defined as a linear combination of a bi-directional mask \mathbf{B} and a causal mask \mathbf{C} . α is the hyper-parameter controlling the mask configuration, *i.e.*, soft mask degenerates into \mathbf{B} or \mathbf{C} when $\alpha = 1$ or $\alpha = 0$, respectively. As illustrated in Figure 3(a), α involves three related hyper-parameters: 1) scheme: how α drops from 1 to 0: we try a linear or a constant scheme. 2) cutoff epochs: when will α drops to 0. 3) learning rate (lr) warmup [26, 19]: this hyper-parameter overlaps with the duration of soft mask. We initially set the lr warmup epochs at 50, consistent with previous settings. When using a linear scheme with 50 and 25 cutoff epochs, we observe an improvement in performance for both iLLaMA-T/16 and iLLaMA-B/16 models, achieving 74.9% and 81.6%, respectively. Ablations are detailed in Section. 4.1. We plot the training curve of the iLLaMA-T/16 in Figure 3(b), using a constant scheme with 50 cutoff epochs. When soft mask ends, we observe that although there was a sharp drop in accuracy, the model ends up achieving better performance. Similar case of the iLLaMA-B/16 are shown in Appendix E. Additionally, we discover that a lower learning rate warmup helps iLLaMA-T/16 achieve 75.0% accuracy, by using a constant scheme with 50 cutoff epochs. However, such approach leads larger iLLaMA-B/16 training to fail to converge. As a result, we only used the lower learning rate warmup for iLLaMA-T/16. Notably, the final training loss within both iLLaMA-T/16 and iLLaMA-B/16 decreases when using soft masks, suggesting a mitigation of the potential underfitting concern.

3.7 Analysis of causal Self-attention

Next, we analyze the advantages of using causal self-attention in iLLaMA, in terms of computational efficiency and expressive ability of visual representation through the lens of attention map rank.

Computational Complexity. We compare the efficiency of causal self-attention and bi-directional baseline. For a self-attention with a sequence length N and embedding dimension D , FLOPs are reported in Table 2 (RoPE is not involved as only attention computations are considered). causal self-attention, in light of the lower triangular property of its attention map, slightly reduces the FLOPs compared to the bi-directional baseline — the degree of reduction grows as sequence length increases.

Attention map rank. We examine the representation learning power of causal attention through a spectrum analysis. Following [60, 48], we perform singular value decomposition on the attention maps of the pre-trained ViT-T/16 and iLLaMA-T/16 models. Next, we sort the singular values and plot a curve illustrating the relationship between the cumulative normalized singular values and matrix indices. The results are conducted using 30 images randomly selected from the ImageNet-1K validation set. As shown in Figure 4, the curve of ViT exhibits concave function characteristics, while the curve of iLLaMA is close to a linear function, indicating a more uniform distribution of singular values in iLLaMA’s attention map. Approximating the matrix rank by the index at which the cumulative normalized singular value reaches 0.8, we observe that the index value of iLLaMA is about 48 higher than that of ViT (~ 129 -th v.s. ~ 81 -th). Under such premise, compared to ViT, the attention map of iLLaMA can be approximated with a certain error by a higher-rank matrix. Accordingly, the rank of the attention map may affect the expressive capabilities of the learned representations [13], suggesting that the causal self-attention in iLLaMA has the potential to learn complex visual representations, as empirically demonstrated in Section 4.2. Detailed results for different layers and heads are provided in Appendix D.

Closing remarks. So far, we have finished the design roadmap of iLLaMA through architectural and training strategy modification. iLLaMA, a decoder-only Transformer, shows advantages in computational complexity and attention map rank through its causal self-attention mechanism. Notably, while all components of iLLaMA are essentially derived from LLaMA, relying only on them is insufficient for an effective weight optimization, as demonstrated in Section 3.3. In fact, the proposed PS [cls] and soft mask strategy effectively address this issue and assist in iLLaMA training. However, to achieve a comprehensive understanding of iLLaMA’s properties, some useful evaluation should be conducted: 1) Scalability for large model capacities (>300 M parameters) and dataset sizes (>10 M training images, *e.g.*, ImageNet-21K). 2) Other practical evaluation dimensions, such as model calibration, shape-texture bias, downstream task performance, quantization compatibility, discussed below.

Table 2: Computational complexity results. causal mask slightly reduces FLOPs required in the self-attention.

Type	Bi-directional	causal
FLOPs	$4ND^2 + 2N^2D$	$4ND^2 + N^2D + (\lfloor N^2/2 \rfloor + 1)D$

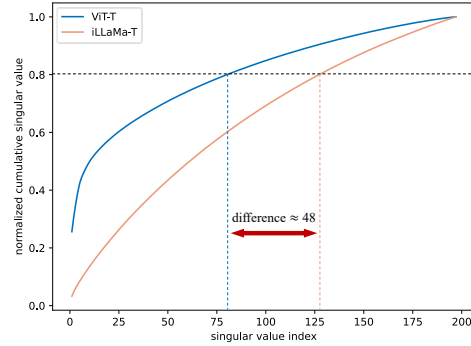


Figure 4: Rank analysis of the attention map in head 1, layer 1 of the pretrained ViT-T and iLLaMA-T with $N = 197$. Difference between them is about 48.

4 Experiments

This section provide a comprehensive evaluation of iLLaMA. We first report ablation results, *e.g.*, the effectiveness of data augmentation and different soft mask strategies. Next, we compare iLLaMA with other strong baselines on ImageNet classification. Beyond ImageNet accuracy, we also examine its efficacy on calibration, shape-texture bias, and evaluate its compatibility with quantization-aware training and downstream task performance.

4.1 Ablation Study

Influence of data augmentation. Base on the observation in Section 3.5, we examined multiple sets of cutmix and mixup settings, as reported in Table 5. We empirically observe that the smaller iLLaMA-T/16 are more sensitive to two data augmentation strategies and perform better with lower hyper-parameters, whereas the larger iLLaMA-B/16 are suited to higher ones. This may be related to the architectural differences between LLaMA’s Transformer decoder and ViT’s encoder type.

Table 3: Soft mask scheduling for iLLaMA-T/16 and iLLaMA-B/16 on ImageNet-1K.

Schedule	Cutoff Epochs	Tiny	Base
no softmask	-	74.3	81.3
linear	25	74.8	81.6
linear	50	74.9	81.5
linear	100	74.9	81.5
constant	25	74.7	81.5
constant	50	74.8	81.5

Table 4: Soft mask for training loss and testing loss. Soft mask lowers both training and testing loss in tiny and base models, counteracting underfitting issue and thus leading to a better optimization.

Model	Training Loss	Testing Loss
tiny	2.990	1.121
+ soft mask	2.955 ($\downarrow 0.045$)	1.092 ($\downarrow 0.029$)
base	2.868	0.843
+ soft mask	2.828 ($\downarrow 0.040$)	0.831 ($\downarrow 0.012$)

Influence of soft mask scheduling strategies and epochs. As mentioned in Section 3.6, the proposed soft mask technique includes three hyper-parameters, *i.e.*, schedule, cutoff epochs and lr warmup epochs. Here we evaluate the robustness of soft mask to hyper-parameter settings, with results detailed in Table 3. Beyond the *linear* schedule, inspired by [36], we also implemented a *constant* option. Additionally, we fixed the learning rate warm-up epochs at 50 and experimented with different cutoff epochs. The results reveal that the soft mask facilitates the optimization of iLLaMA under both linear and constant scheduling, suitable for models of both tiny and base sizes. Moreover, setting the cutoff epochs to span a wide range from 25 to 100 is advantageous. Notably, the soft mask can be easily integrated into existing code frameworks (*e.g.*, timm [62]) with negligible additional training costs, thereby facilitating its effortless application on future related architectures.

Influence of soft mask for training and testing loss.

A common challenge deep neural networks encounter is underfitting [36], often characterized by the difficulty in continuously reducing training loss during model training and resulting in unsatisfactory test accuracy. We compare the training and testing losses of the iLLaMA-T/16 and iLLaMA-B/16 models with and without the use of the soft mask strategy, as shown in Table 4. We observe that soft mask can reduce training loss in both regimes, mitigating potential underfitting issue and reducing testing loss.

Table 5: Mixup and cutmix ablation results.

Mixup	Cutmix	Tiny	Mixup	Cutmix	Base
0.8	1.0	73.2	0.8	1.0	81.2
0.5	0.4	73.8	0.9	0.9	81.2
0.3	0.3	73.9	0.9	1.0	81.2
0.2	0.2	74.3	1.0	1.0	81.2
0.1	0.1	74.3	0.95	1.0	81.3

4.2 Comparison with Recent Architectures on ImageNet-1K Classification

We conducted experiments on the ImageNet-1K [11] benchmark with different model sizes (*i.e.*, iLLaMA-T/S/B/L) to examine its scalability. Detailed architecture configurations are in Appendix A.

ImageNet-1K training. ImageNet-1K dataset contains 1281167 training images and 50000 testing images from 1000 classes. We train iLLaMA-T/S/B on ImageNet-1K for 300 epochs with AdamW optimizer [37] and a batch size of 4096. The ImageNet-1K trained iLLaMA-T/B models are, in fact, the outcome of the explorations completed in Section 3.6. For the settings of soft mask schedule, cutoff epochs, and learning rate warmup epochs, we tune slightly for the iLLaMA-S model.

ImageNet-21K pre-training. We use the ‘Winter21 variant of ImageNet-21K-P’ (referred to as ImageNet-21K) dataset [43]² for large-scale pre-training, which contains 11060223 training images and 522500 testing images from 10450 classes. Only the train set was used. We pre-train iLLaMA-B/L on ImageNet-21K for 90 epochs using a constant soft mask schedule, with cutoff epochs and learning rate warmup epochs set to 30 and 5, respectively. Detailed recipes can be found in Appendix B.2.

ImageNet-1K fine-tuning. We fine-tune the iLLaMA-B model, trained on ImageNet-1K, at a resolution of 384×384 . Similarly, the iLLaMA-B/L model, trained on ImageNet-21K, was fine-tuned at resolutions of 224×224 and 384×384 , respectively. All fine-tuning was conducted for 30 epochs using the AdamW optimizer. We follow DeiT [51] for interpolating positional embeddings to allow our iLLaMA to handle inputs at a higher resolution. Other settings are detailed in Appendix B.3.

Results. Table 6 shows a comparison between iLLaMA and other strong visual baselines, including ConvNets (ConvNeXt [35], ConvNeXt-V2 [63]), vision Transformers (ViT [14], Swin Transformer [34]), MLPs (PoolFormer [66], VanillaNet [5]), and recent language model inspired models (AIM [15], VisionLLaMA [9]). We present three observations: 1) The performance-parameter trade-off of iLLaMA surpasses other LM-inspired models such as AIM and VisionLLaMA, presumably

²downloaded from: <https://www.image-net.org/download-images.php>

Table 6: ImageNet-1K accuracy. Throughput (images/s) are tested on Nvidia A100 GPU with a batch size of 1024. Hie.: Hierarchical, Iso.: Isotropic, Sup.: Supervised (pre-)training, AR.: Autoregressive pre-training. ♠ ConvNet, ■ Vision Transformer, ♣ MLP, ✧ LM-inspired visual model, ★ LLaMA.

Model	Dataset Used	Objective	Type	Image Size	Params	MACs	Throughput	Acc
♠ ConvNeXt-S [35]	IN-1K	Sup.	Hie.	224×224	50M	8.7G	1185	83.1
♠ ConvNeXt-B [35]	IN-1K	Sup.	Hie.	224×224	89M	15.4G	877	83.8
♠ ConvNeXt-L [35]	IN-1K	Sup.	Hie.	224×224	198M	34.4G	543	84.3
♠ ConvNeXtV2-N [63]	IN-1K	Sup.	Hie.	224×224	15.6M	2.45G	2120	81.2
♠ ConvNeXtV2-T [63]	IN-1K	Sup.	Hie.	224×224	28.6M	4.47G	1362	82.5
♠ ConvNeXtV2-B [63]	IN-1K	Sup.	Hie.	224×224	88.7M	15.4G	645	84.3
■ Swin-S [34]	IN-1K	Sup.	Hie.	224×224	50M	8.7G	934	83.0
■ Swin-B [34]	IN-1K	Sup.	Hie.	224×224	88M	15.4G	710	83.5
■ DeiT-Ti [51]	IN-1K	Sup.	Iso.	224×224	5.7M	1.3G	6051	72.2
■ DeiT-S [51]	IN-1K	Sup.	Iso.	224×224	22.1M	4.6G	3080	79.8
■ DeiT-B [51]	IN-1K	Sup.	Iso.	224×224	86.4M	17.6G	1348	81.8
■ ViT-B/16 [14]	IN-21K, IN-1K	Sup., Sup.	Iso.	384×384	86.4M	55.5G	349	84.0
■ ViT-L/16 [14]	IN-21K, IN-1K	Sup., Sup.	Iso.	384×384	304.1M	191.2G	124	85.2
♣ PoolFormer-S12 [66]	IN-1K	Sup.	Hie.	224×224	12M	1.8G	4354	77.2
♣ PoolFormer-M48 [66]	IN-1K	Sup.	Hie.	224×224	73M	11.6G	768	82.5
♣ VanillaNet-5 [5]	IN-1K	Sup.	Hie.	224×224	15.5M	5.2G	-	72.5
♣ VanillaNet-13-1.5×[5]	IN-1K	Sup.	Hie.	224×224	127.8M	26.5G	-	82.5
✧ AIM-0.6B [15]	DFN-2B+, IN-1K	AR., Sup.	Iso.	224×224	0.6B	-	-	78.5
✧ AIM-3B [15]	DFN-2B+, IN-1K	AR., Sup.	Iso.	224×224	3B	-	-	82.2
✧ AIM-7B [15]	DFN-2B+, IN-1K	AR., Sup.	Iso.	224×224	7B	-	-	82.4
✧ P-VisionLLaMA-S [9]	IN-1K	Sup.	Hie.	224×224	24M	-	-	81.6
✧ P-VisionLLaMA-B [9]	IN-1K	Sup.	Hie.	224×224	56M	-	-	83.2
✧ P-VisionLLaMA-L [9]	IN-1K	Sup.	Hie.	224×224	99M	-	-	83.6
✧ VisionLLaMA-L [9]	IN-1K, IN-1K	Sup., Sup.	Iso.	224×224	310M	-	-	84.6
★ iLLaMA-T	IN-1K	Sup.	Iso.	224×224	5.7M	1.3G	6958	75.0
★ iLLaMA-S	IN-1K	Sup.	Iso.	224×224	21.9M	4.6G	3222	79.9
★ iLLaMA-B	IN-1K	Sup.	Iso.	224×224	86.3M	17.6G	1345	81.6
★ iLLaMA-B	IN-1K	Sup.	Iso.	384×384	86.3M	55.5G	332	83.0
★ iLLaMA-B	IN-21K, IN-1K	Sup., Sup.	Iso.	224×224	86.3M	17.6G	1345	83.6
★ iLLaMA-B	IN-21K, IN-1K	Sup., Sup.	Iso.	384×384	86.3M	55.5G	332	85.0
★ iLLaMA-L	IN-21K, IN-1K	Sup., Sup.	Iso.	224×224	310.2M	62.8G	456	84.8
★ iLLaMA-L	IN-21K, IN-1K	Sup., Sup.	Iso.	384×384	310.2M	194.7G	116	86.0

due to its use of causal attention and soft mask training techniques. 2) iLLaMA exhibits a superior accuracy-throughput trade-off compared to strong hierarchical baselines such as ConvNeXt-V2-N/T/B and Swin-S/B. We attribute this to iLLaMA’s isotropic design (each intermediate block has the same feature resolution), which benefits from a straightforward and efficient architecture, enhancing inference speed. 3) Scalability of model capacity and dataset size: After comprehensive pre-training on the expanded ImageNet-21K dataset, the iLLaMA-B model achieves more than 85.0% accuracy on ImageNet-1K with under 100M parameters, significantly outperforming ViT-B’s 84.0%. Upon scaling up to the larger iLLaMA-L, accuracy reaches 86.0%, exceeding that of ViT-L pre-trained on ImageNet-21K and the AIM-7B pre-trained on the DFN-2B+ dataset. To our knowledge, this showcases SOTA performance for LLaMA-type architectures.

4.3 Model Calibration and Shape-Texture Bias

Beyond ImageNet accuracy, we also examined iLLaMA’s calibration properties and shape-texture bias for a more detailed evaluation, following [59]. Besides iLLaMA, we also explore two prevalent architectures, *i.e.*, ConvNeXt [35] and DeiT3 [52], representing ConvNets and Transformers, respectively. We apply ImageNet-21K pre-trained and ImageNet-1K fine-tuned models in this section.

Model calibration. Model calibration represents the relationship between a model’s precision and confidence across samples of varying difficulty, *i.e.*, poor-calibrated models tend to produce overly confident yet incorrect predictions, whereas well-calibrated models demonstrate a strong correlation between confidence and accuracy [22]. Calibration is commonly measured using the Expected Calibration Error (ECE), where a lower ECE is favorable. ECE results for different models on

Table 7: Quantization results. #Bits (w-a): w bit weights, a bit activations. 8-bit iLLaMA-T matches 32-bit DeiT-T.

Model	#Bits	Tiny	Small
DeiT [51]	32-32	72.2	79.8
iLLaMA	32-32	75.0	79.9
iLLaMA	8-8	72.4	77.4

Table 9: Soft mask for CIFAR transfer learning. Soft mask improves iLLaMA performance without changing the inference architecture.

Model	CIFAR10	CIFAR100
ViT-T	98.0	85.5
iLLaMA-T	97.9	84.8
+ soft mask	97.9	85.5

Table 8: Calibration (expected calibration error \downarrow) and shape-texture bias (ratio \uparrow) results of ConvNeXt-B [35], DeiT3-B [52] and iLLaMA-B. We use both IN-21K pre-trained and IN-1K fine-tuned models.

Evaluation	ConvNeXt-B	DeiT3-B	iLLaMA-B
Calibration	0.0281	0.0415	0.0335
Shape-Texture Bias	33.30%	39.86%	41.45%

Table 10: ADE20K semantic segmentation results using UperNet [64]. We report mIoU with multi-scale testing. FLOPs calculation are based on input sizes of (512, 512).

Backbone	Input Crop.	mIoU	#Param.	FLOPs
ViT-T	512 ²	39.8	10.88M	37.1G
iLLaMA-T	512 ²	37.7	10.86M	37.1G
ViT-B	512 ²	47.3	163.29M	585.7G
iLLaMA-B	512 ²	45.1	163.22M	585.7G

ImageNet-1K are presented in Table 8. The calibration of iLLaMA is lower than that of DeiT3, suggesting that the output confidence of iLLaMA is more reliable. We also plot the reliability diagrams [59] to intuitively compare the calibration of different models, detailed in Appendix F.

Shape-texture bias. Shape-texture bias measures the extent to which the model relies on the shape or texture of the image when performing recognition [18]. We generally prefer models to mimic human eye behavior, relying more on shape rather than texture [55, 17]. We calculate the shape ratio for all models on cue-conflict images and report the results in Table 8, following [59]. Our iLLaMA shows the largest shape ratio of 41.45% among the three compared baselines, suggesting the potential of the LLM architecture for vision. Detailed results can be found in Appendix G.

4.4 Compatibility with Quantization

Since a practical goal for neural networks is deployment on low-bit hardware chips, we further examine iLLaMA’s compatibility with quantization. We basically follow Q-ViT [33] to apply quantization-aware training (QAT) to iLLaMA, with weights and activations of all blocks’ FFN and causal self-attention layers to 8 bits. Quantization recipes and results are shown in Appendix B.4 and Table 7, respectively. Different sizes of low-bit iLLaMA maintain accuracy well, and 8-bit iLLaMA-T is even compete favorably with the full-precision DeiT-T [51] (72.4% v.s. 72.2%).

4.5 Transferability on Downstream Tasks

CIFAR transfer learning. We fine-tune ViT-T and iLLaMA-T on the CIFAR datasets [31], including an ablation of the soft mask on iLLaMA. Detailed recipes are provided in Appendix B.5. iLLaMA’s performance on CIFAR datasets is essentially on par with ViT, assuring that iLLaMA can be confidently applied in the transfer learning field as a practical alternative to ViT. Additionally, soft mask is helpful in the relatively complicated CIFAR100, demonstrating its generalizability.

ADE20K semantic segmentation. We fine-tune our ImageNet-1K pre-trained iLLaMA and ViT models on ADE20K [72] dataset using UperNet [64] to perform semantic segmentation task. For both iLLaMA and ViT, we set the learning rate as 6e-5 and weight decay as 0.01. Table 10 presents the results. iLLaMA’s performance is marginally lower than ViT’s, which we attribute to the potential impact of the masking mechanism in iLLaMA’s causal attention on high-resolution dense prediction tasks. This suggests there is still space for optimization, a subject for future investigation.

5 Conclusions

In the general trend of using encoder to build vision architectures, the suitability for decoder-only architecture still exists a research gap. We systematically studies whether decoder, an architecture that has shown amazing potential in LLMs, can also take root in learning visual representation through visual supervised training. The key component – causal self-attention we used – is not novel and is

inherited from existing LLM architectures, but we propose pivotal techniques, *i.e.*, PS [cls] and soft mask, to effectively adapt them to visual tasks. We hope that this work will inspire more exploration towards a generic pure decoder architecture that fully unifies vision and text.

References

- [1] Jimmy Lei Ba, Jamie Ryan Kiros, and Geoffrey E Hinton. Layer normalization. *arXiv preprint arXiv:1607.06450*, 2016.
- [2] Yutong Bai, Xinyang Geng, Karttikeya Mangalam, Amir Bar, Alan Yuille, Trevor Darrell, Jitendra Malik, and Alexei A Efros. Sequential modeling enables scalable learning for large vision models. *arXiv preprint arXiv:2312.00785*, 2023.
- [3] Hangbo Bao, Li Dong, Songhao Piao, and Furu Wei. Beit: Bert pre-training of image transformers. In *ICLR*, 2021.
- [4] William Chan, Nikita Kitaev, Kelvin Guu, Mitchell Stern, and Jakob Uszkoreit. Kermit: Generative insertion-based modeling for sequences. *arXiv preprint arXiv:1906.01604*, 2019.
- [5] Hanting Chen, Yunhe Wang, Jianyuan Guo, and Dacheng Tao. Vanillanet: the power of minimalism in deep learning. In *NeurIPS*, 2023.
- [6] Mark Chen, Alec Radford, Rewon Child, Jeffrey Wu, Heewoo Jun, David Luan, and Ilya Sutskever. Generative pretraining from pixels. In *ICML*, 2020.
- [7] Wei-Lin Chiang, Zhuohan Li, Zi Lin, Ying Sheng, Zhanghao Wu, Hao Zhang, Lianmin Zheng, Siyuan Zhuang, Yonghao Zhuang, Joseph E. Gonzalez, Ion Stoica, and Eric P. Xing. Vicuna: An open-source chatbot impressing gpt-4 with 90%* chatgpt quality, March 2023.
- [8] Aakanksha Chowdhery, Sharan Narang, Jacob Devlin, Maarten Bosma, Gaurav Mishra, Adam Roberts, Paul Barham, Hyung Won Chung, Charles Sutton, Sebastian Gehrmann, et al. Palm: Scaling language modeling with pathways. *arXiv preprint arXiv:2204.02311*, 2022.
- [9] Xiangxiang Chu, Jianlin Su, bo Zhang, and Chunhua Shen. Visionllama: A unified llama interface for vision tasks. *arXiv preprint arXiv:2403.00522*, 2024.
- [10] Ekin D Cubuk, Barret Zoph, Jonathon Shlens, and Quoc V Le. Randaugment: Practical automated data augmentation with a reduced search space. In *CVPR Workshops*, 2020.
- [11] Jia Deng, Wei Dong, Richard Socher, Li-Jia Li, Kai Li, and Li Fei-Fei. Imagenet: A large-scale hierarchical image database. In *CVPR*, 2009.
- [12] Jacob Devlin, Ming-Wei Chang, Kenton Lee, and Kristina Toutanova. Bert: Pre-training of deep bidirectional transformers for language understanding. In *NAACL*, 2019.
- [13] Yihe Dong, Jean-Baptiste Cordonnier, and Andreas Loukas. Attention is not all you need: Pure attention loses rank doubly exponentially with depth. In *ICML*, 2021.
- [14] Alexey Dosovitskiy, Lucas Beyer, Alexander Kolesnikov, Dirk Weissenborn, Xiaohua Zhai, Thomas Unterthiner, Mostafa Dehghani, Matthias Minderer, Georg Heigold, Sylvain Gelly, et al. An image is worth 16x16 words: Transformers for image recognition at scale. In *ICLR*, 2020.
- [15] Alaaeldin El-Nouby, Michal Klein, Shuangfei Zhai, Miguel Angel Bautista, Alexander Toshev, Vaishal Shankar, Joshua M Susskind, and Armand Joulin. Scalable pre-training of large autoregressive image models. *arXiv preprint arXiv:2401.08541*, 2024.
- [16] Stefan Elfving, Eiji Uchibe, and Kenji Doya. Sigmoid-weighted linear units for neural network function approximation in reinforcement learning. *Neural networks*, 2018.
- [17] Robert Geirhos, Jörn-Henrik Jacobsen, Claudio Michaelis, Richard Zemel, Wieland Brendel, Matthias Bethge, and Felix A Wichmann. Shortcut learning in deep neural networks. *Nature Machine Intelligence*, 2020.
- [18] Robert Geirhos, Patricia Rubisch, Claudio Michaelis, Matthias Bethge, Felix A Wichmann, and Wieland Brendel. Imagenet-trained cnns are biased towards texture; increasing shape bias improves accuracy and robustness. *arXiv preprint arXiv:1811.12231*, 2018.
- [19] Priya Goyal, Piotr Dollár, Ross Girshick, Pieter Noordhuis, Lukasz Wesolowski, Aapo Kyrola, Andrew Tulloch, Yangqing Jia, and Kaiming He. Accurate, large minibatch sgd: Training imagenet in 1 hour. *arXiv preprint arXiv:1706.02677*, 2017.
- [20] Jiatao Gu, James Bradbury, Caiming Xiong, Victor OK Li, and Richard Socher. Non-autoregressive neural machine translation. In *ICLR*, 2018.
- [21] Jiatao Gu, Changhan Wang, and Junbo Zhao. Levenshtein transformer. In *NeurIPS*, 2019.

- [22] Chuan Guo, Geoff Pleiss, Yu Sun, and Kilian Q Weinberger. On calibration of modern neural networks. In *ICML*, 2017.
- [23] Jianyuan Guo, Kai Han, Han Wu, Yehui Tang, Xinghao Chen, Yunhe Wang, and Chang Xu. Cmt: Convolutional neural networks meet vision transformers. In *CVPR*, 2022.
- [24] Jianyuan Guo, Zhiwei Hao, Chengcheng Wang, Yehui Tang, Han Wu, Han Hu, Kai Han, and Chang Xu. Data-efficient large vision models through sequential autoregression. *arXiv preprint arXiv:2402.04841*, 2024.
- [25] Kaiming He, Xinlei Chen, Saining Xie, Yanghao Li, Piotr Dollár, and Ross Girshick. Masked autoencoders are scalable vision learners. In *CVPR*, 2022.
- [26] Kaiming He, Xiangyu Zhang, Shaoqing Ren, and Jian Sun. Deep residual learning for image recognition. In *CVPR*, 2016.
- [27] Dan Hendrycks and Kevin Gimpel. Gaussian error linear units (gelus). *arXiv preprint arXiv:1606.08415*, 2016.
- [28] Geoffrey E Hinton, Nitish Srivastava, Alex Krizhevsky, Ilya Sutskever, and Ruslan R Salakhutdinov. Improving neural networks by preventing co-adaptation of feature detectors. *arXiv preprint arXiv:1207.0580*, 2012.
- [29] Gao Huang, Yu Sun, Zhuang Liu, Daniel Sedra, and Kilian Q Weinberger. Deep networks with stochastic depth. In *ECCV*, 2016.
- [30] Albert Q Jiang, Alexandre Sablayrolles, Arthur Mensch, Chris Bamford, Devendra Singh Chaplot, Diego de las Casas, Florian Bressand, Gianna Lengyel, Guillaume Lample, Lucile Saulnier, et al. Mistral 7b. *arXiv preprint arXiv:2310.06825*, 2023.
- [31] Alex Krizhevsky, Geoffrey Hinton, et al. Learning multiple layers of features from tiny images. 2009.
- [32] Hao Li, Zheng Xu, Gavin Taylor, Christoph Studer, and Tom Goldstein. Visualizing the loss landscape of neural nets. In *Advances in neural information processing systems*, 2018.
- [33] Yanjing Li, Sheng Xu, Baohang Zhang, Xianbin Cao, Peng Gao, and Guodong Guo. Q-vit: Accurate and fully quantized low-bit vision transformer. In *NeurIPS*, 2022.
- [34] Ze Liu, Yutong Lin, Yue Cao, Han Hu, Yixuan Wei, Zheng Zhang, Stephen Lin, and Baining Guo. Swin transformer: Hierarchical vision transformer using shifted windows. In *ICCV*, 2021.
- [35] Zhuang Liu, Hanzi Mao, Chao-Yuan Wu, Christoph Feichtenhofer, Trevor Darrell, and Saining Xie. A convnet for the 2020s. In *CVPR*, 2022.
- [36] Zhuang Liu, Zhiqiu Xu, Joseph Jin, Zhiqiang Shen, and Trevor Darrell. Dropout reduces underfitting. In *ICML*, 2023.
- [37] Ilya Loshchilov and Frank Hutter. Decoupled weight decay regularization. In *ICLR*, 2019.
- [38] Aaron van den Oord, Sander Dieleman, Heiga Zen, Karen Simonyan, Oriol Vinyals, Alex Graves, Nal Kalchbrenner, Andrew Senior, and Koray Kavukcuoglu. Wavenet: A generative model for raw audio. *arXiv preprint arXiv:1609.03499*, 2016.
- [39] Ziqi Pang, Ziyang Xie, Yunze Man, and Yu-Xiong Wang. Frozen transformers in language models are effective visual encoder layers. *arXiv preprint arXiv:2310.12973*, 2023.
- [40] Boris T Polyak and Anatoli B Juditsky. Acceleration of stochastic approximation by averaging. *SIAM journal on control and optimization*, 1992.
- [41] Prajit Ramachandran, Barret Zoph, and Quoc V Le. Searching for activation functions. In *ICLR Workshop*, 2018.
- [42] Ali Razavi, Aaron Van den Oord, and Oriol Vinyals. Generating diverse high-fidelity images with vq-vae-2. In *NeurIPS*, 2019.
- [43] Tal Ridnik, Emanuel Ben-Baruch, Asaf Noy, and Lihi Zelnik-Manor. Imagenet-21k pretraining for the masses. *arXiv preprint arXiv:2104.10972*, 2021.
- [44] Baptiste Roziere, Jonas Gehring, Fabian Gloeckle, Sten Sootla, Itai Gat, Xiaoqing Ellen Tan, Yossi Adi, Jingyu Liu, Tal Remez, Jérémy Rapin, et al. Code llama: Open foundation models for code. *arXiv preprint arXiv:2308.12950*, 2023.
- [45] Chitwan Saharia, William Chan, Saurabh Saxena, and Mohammad Norouzi. Non-autoregressive machine translation with latent alignments. *arXiv preprint arXiv:2004.07437*, 2020.
- [46] Tim Salimans, Andrej Karpathy, Xi Chen, and Diederik P Kingma. Pixelcnn++: Improving the pixelcnn with discretized logistic mixture likelihood and other modifications. *arXiv preprint arXiv:1701.05517*, 2017.
- [47] Noam Shazeer. Glu variants improve transformer. *arXiv preprint arXiv:2002.05202*, 2020.

- [48] Han Shu, Jiahao Wang, Hanting Chen, Lin Li, Yujiu Yang, and Yunhe Wang. Adder attention for vision transformer. In *NeurIPS*, 2021.
- [49] Jianlin Su, Murtadha Ahmed, Yu Lu, Shengfeng Pan, Wen Bo, and Yunfeng Liu. Roformer: Enhanced transformer with rotary position embedding. *Neurocomputing*, 2024.
- [50] Christian Szegedy, Vincent Vanhoucke, Sergey Ioffe, Jon Shlens, and Zbigniew Wojna. Rethinking the inception architecture for computer vision. In *CVPR*, 2016.
- [51] Hugo Touvron, Matthieu Cord, Matthijs Douze, Francisco Massa, Alexandre Sablayrolles, and Hervé Jégou. Training data-efficient image transformers & distillation through attention. In *ICML*, 2021.
- [52] Hugo Touvron, Matthieu Cord, and Hervé Jégou. Deit iii: Revenge of the vit. In *ECCV*, 2022.
- [53] Hugo Touvron, Thibaut Lavril, Gautier Izacard, Xavier Martinet, Marie-Anne Lachaux, Timothée Lacroix, Baptiste Rozière, Naman Goyal, Eric Hambro, Faisal Azhar, et al. Llama: Open and efficient foundation language models. *arXiv preprint arXiv:2302.13971*, 2023.
- [54] Hugo Touvron, Louis Martin, Kevin Stone, Peter Albert, Amjad Almahairi, Yasmine Babaei, Nikolay Bashlykov, Soumya Batra, Prajjwal Bhargava, Shruti Bhosale, et al. Llama 2: Open foundation and fine-tuned chat models. *arXiv preprint arXiv:2307.09288*, 2023.
- [55] Shikhar Tuli, Ishita Dasgupta, Erin Grant, and Thomas L Griffiths. Are convolutional neural networks or transformers more like human vision? *arXiv preprint arXiv:2105.07197*, 2021.
- [56] Aaron Van Den Oord, Nal Kalchbrenner, Lasse Espeholt, Oriol Vinyals, Alex Graves, et al. Conditional image generation with pixelcnn decoders. 2016.
- [57] Aäron Van Den Oord, Nal Kalchbrenner, and Koray Kavukcuoglu. Pixel recurrent neural networks. In *ICML*, 2016.
- [58] Ashish Vaswani, Noam Shazeer, Niki Parmar, Jakob Uszkoreit, Llion Jones, Aidan N Gomez, Lukasz Kaiser, and Illia Polosukhin. Attention is all you need. In *NIPS*, 2017.
- [59] Kirill Vishniakov, Zhiqiang Shen, and Zhuang Liu. Convnet vs transformer, supervised vs clip: Beyond imagenet accuracy. *arXiv preprint arXiv:2311.09215*, 2023.
- [60] Sinong Wang, Belinda Z Li, Madian Khabsa, Han Fang, and Hao Ma. Linformer: Self-attention with linear complexity. *arXiv preprint arXiv:2006.04768*, 2020.
- [61] Wenhai Wang, Enze Xie, Xiang Li, Deng-Ping Fan, Kaitao Song, Ding Liang, Tong Lu, Ping Luo, and Ling Shao. Pyramid vision transformer: A versatile backbone for dense prediction without convolutions. In *ICCV*, 2021.
- [62] Ross Wightman. Pytorch image models. <https://github.com/rwightman/pytorch-image-models>, 2019.
- [63] Sanghyun Woo, Shoubhik Debnath, Ronghang Hu, Xinlei Chen, Zhuang Liu, In So Kweon, and Saining Xie. Convnext v2: Co-designing and scaling convnets with masked autoencoders. In *CVPR*, 2023.
- [64] Tete Xiao, Yingcheng Liu, Bolei Zhou, Yuning Jiang, and Jian Sun. Unified perceptual parsing for scene understanding. In *ECCV*, 2018.
- [65] Zhiqiu Xu, Yanjie Chen, Kirill Vishniakov, Yida Yin, Zhiqiang Shen, Trevor Darrell, Lingjie Liu, and Zhuang Liu. Initializing models with larger ones. In *ICLR*, 2024.
- [66] Weihao Yu, Mi Luo, Pan Zhou, Chenyang Si, Yichen Zhou, Xinchao Wang, Jiashi Feng, and Shuicheng Yan. Metaformer is actually what you need for vision. In *CVPR*, 2022.
- [67] Sangdoo Yun, Dongyoon Han, Seong Joon Oh, Sanghyuk Chun, Junsuk Choe, and Youngjoon Yoo. Cutmix: Regularization strategy to train strong classifiers with localizable features. In *ICCV*, 2019.
- [68] Biao Zhang and Rico Sennrich. Root mean square layer normalization. In *NeurIPS*, 2019.
- [69] Hongyi Zhang, Moustapha Cisse, Yann N Dauphin, and David Lopez-Paz. mixup: Beyond empirical risk minimization. In *ICLR*, 2018.
- [70] Susan Zhang, Stephen Roller, Naman Goyal, Mikel Artetxe, Moya Chen, Shuohui Chen, Christopher Dewan, Mona Diab, Xian Li, Xi Victoria Lin, et al. Opt: Open pre-trained transformer language models, 2022. *arXiv preprint arXiv:2205.01068*, 2023.
- [71] Zhun Zhong, Liang Zheng, Guoliang Kang, Shaozi Li, and Yi Yang. Random erasing data augmentation. In *AAAI*, 2020.
- [72] Bolei Zhou, Hang Zhao, Xavier Puig, Tete Xiao, Sanja Fidler, Adela Barriuso, and Antonio Torralba. Semantic understanding of scenes through the ade20k dataset. *IJCV*, 2019.
- [73] Chunting Zhou, Graham Neubig, and Jiatao Gu. Understanding knowledge distillation in non-autoregressive machine translation. In *ICLR*, 2020.

Appendix

In this Appendix, we detail our network configuration (§A), outline experimental recipe to replicate our study (§B), share insights from the iLLaMA exploration (§C), , and analyze both the causal self-attention (§D) and soft mask techniques (§E). Additionally, we explore iLLaMA’s calibration property (§F), shape-texture bias (§G), loss landscape (§H), its limitations (§I), and its potential societal impacts (§J).

A Network Configuration

In Table 11, we provide detailed architecture configurations for iLLaMA models of various capacities. Our approach to scaling up the model size, from small to large, is similar to that of the ViT. Thus, akin to ViT, iLLaMA benefits from the simplicity of an isotropic architecture and high throughput, with its internal features remaining unchanged in resolution and number of channel as the depth increases.

We provide a block-level comparison between iLLaMA and ViT model in Figure 5. VisionLLaMA uses SwiGLU, and AS2D RoPE to build LLaMA-style architecture. Differently, we further uses RMSNorm, modified causal self-attention and 1D RoPE from LLaMA to replace layer normalization, bi-directional self-attention, and proposes two pivotal strategies, *i.e.*, *PS [cls]* and *soft mask* to help the optimization of our iLLaMA. We also keep the learnable positional embedding as ViT does.

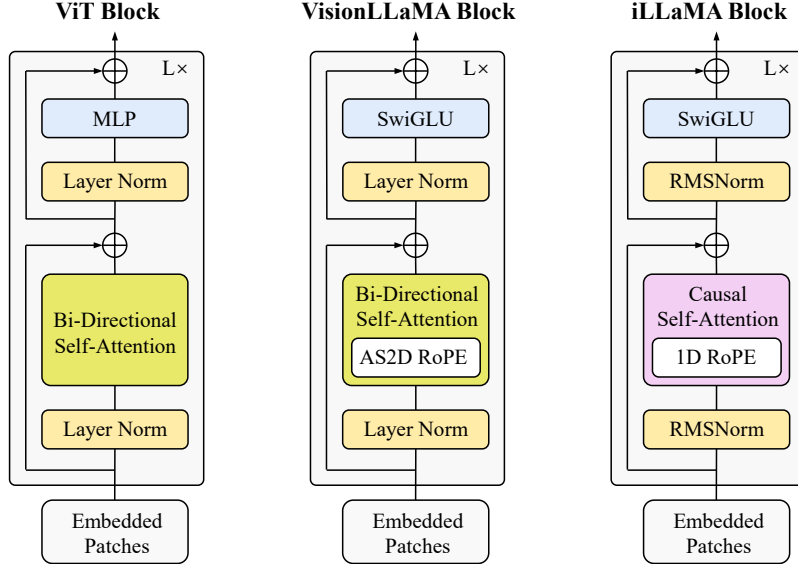


Figure 5: Comparison between ViT [14], VisionLLaMA [9], and iLLaMA blocks.

B Experimental Settings

B.1 Training Recipe in Section 3

Our training recipe for training the tiny and base models during the “designing iLLaMA: a roadmap” (Section 3) is primarily adapted from ConvNeXt [35, 36], summarized in Table 12.

Basically, both regimes use the same experimental setup, with the only difference being the stochastic depth rate at 0.0 and 0.4, respectively. Notably, for the ViT baseline, our experimen-

Table 11: Detailed iLLaMA architecture configurations.

	Tiny (T)	Small (S)	Base (B)	Large (L)
depth	12	12	12	24
embedding dim	192	384	768	1024
number of heads	3	6	12	16
#param. (M)	5.7	21.9	86.3	310.2
MACs (G)	1.3	4.6	17.6	62.8

tal results are 73.8% and 81.5%, as shown in Table 17, which slightly differ from the results of 73.9% and 81.6% reported in [36].

Utilizing only the basic training recipe with architectural modifications, the performance of iLLaMA’s tiny and base models achieves 73.2% and 81.2%, as shown in Table 17, yet remains below the ViT baseline. We attribute this to the impairing effect of causal self-attention on the information mixing among tokens. Thus, we enhance the training recipe, detailed next.

Table 12: Our training recipe for Section 3 in the main paper, adapted from [36].

Training Configuration	iLLaMA-T/B
<i>Initialization:</i> weight init	trunc. normal (0.2)
<i>Training recipe:</i> optimizer optimizer momentum	AdamW [37] $\beta_1, \beta_2=0.9, 0.999$
<i>Learning hyper-parameters:</i> base learning rate learning rate schedule weight decay batch size training epochs lr warmup epochs warmup schedule gradient clip exp. mov. avg. (EMA) [40]	4e-3 cosine decay 0.05 4096 300 50 linear None None
<i>Dropout:</i> dropout rate [28] stochastic depth rate [29]	0.0 0.0/0.4
<i>Data augmentation:</i> input resolution randAugment [10] random erasing [71] label smoothing [50] mixup [69] cutmix [67]	224 ² (9, 0.5) 0.25 0.1 0.8 1.0

B.2 ImageNet (Pre-)training Recipe

As illustrated in Table 13, we provide the detailed ImageNet-1K training hyper-parameters and ImageNet-21K pre-training hyper-parameters for the experimental results in Table 6.

For the iLLaMA-T/S/B models, we train directly on ImageNet-1K and discover that models of different sizes are suited to different soft mask settings. For instance, the soft mask schedules are set to constant/linear/linear, respectively, with cutoff epochs designated as 50/50/25.

We pre-trained the iLLaMA-B/L models on ImageNet-21K for 90 epochs, adhering to the practices in [35]. We set the cutoff epochs to 30, indicating that the iLLaMA models’ self-attention fully transitions to causal self-attention after 30 epochs.

B.3 ImageNet Fine-tuning Recipe

We present the results of fine-tuning models pre-trained on ImageNet-1K at a resolution of 384×384 , as well as the outcomes of fine-tuning models pre-trained on ImageNet-21K at resolutions of 224×224 and 384×384 , as shown in Table 14. All ImageNet-1K fine-tuning experiments were conducted for 30 epochs, following the convention in [35].

For the iLLaMA-B model pre-trained on ImageNet-1K, we used a relatively higher stochastic depth rate of 0.8. For the iLLaMA-B/L models pre-trained on ImageNet-21K, we employed relatively lower stochastic depth rates of 0.2 and 0.3, respectively.

Table 13: Our (pre-)training settings for iLLaMa model on ImageNet-1K/ImageNet-21K, respectively, adapted from [36]. Some key training techniques are highlighted .

(Pre-)Training Configuration	iLLaMA-T/S/B ImageNet-1K	iLLaMA-B/L ImageNet-21K
<i>Initialization:</i> weight init	trunc. normal (0.2)	trunc. normal (0.2)
<i>Training recipe:</i> optimizer optimizer momentum	AdamW $\beta_1, \beta_2=0.9, 0.999$	AdamW $\beta_1, \beta_2=0.9, 0.999$
<i>Learning hyper-parameters:</i> base learning rate learning rate schedule weight decay batch size training epochs warmup schedule gradient clip exp. mov. avg. (EMA)	4e-3 cosine decay 0.05 4096 300 linear None None	1e-3 cosine decay 0.01 4096 90 linear None None
<i>Dropout:</i> dropout rate stochastic depth rate	0.0 0.0/0.1/0.4	0.0 0.1
<i>Data augmentation:</i> input resolution randAugment random erasing label smoothing mixup cutmix	224 ² (9, 0.5) 0.25 0.1 0.1/0.5/0.95 0.1/0.5/1.0	224 ² (9, 0.5) 0.25 0.1 0.8 1.0
<i>Soft mask:</i> soft mask schedule cutoff epochs lr warmup epochs	constant/linear/linear 50/50/25 5/5/50	constant 30 5

Additionally, we standardized the cutoff epoch at 0 for our ImageNet-1K fine-tuning experiments, ensuring the application of a causal mask in self-attention to align with the LLaMA architecture. We also opted not to use learning rate warmup.

B.4 Quantization-aware Training Recipe

We provide our quantization-aware training recipe for iLLaMA in Table 15. Basically we follow the Q-ViT method proposed in [33], with only weights and activations in each basic block’s causal self-attention and FFN module are quantized to 8 bit width.

B.5 CIFAR Transfer Learning Recipe

We further provide our training recipe for transfer learning on the CIFAR10 and CIFAR100 datasets, as shown in Table 16.

In our transfer learning experiments, we consistently apply a linear soft mask schedule. However, for the CIFAR10 and CIFAR100 datasets, we use cutoff epochs of 25 and 50, respectively.

C Designing iLLaMA: detailed results

We present the comprehensive experimental results of our exploration journey of iLLaMA in Table 17. This table not only delineates the stepwise accuracy of both the tiny and base models, as depicted in

Table 14: Our fine-tuning settings for iLLaMa model on ImageNet-1K, adapted from [36]. Some key training techniques are highlighted .

(Pre-)Training Configuration	iLLaMA-B ImageNet-1K 224 ²	iLLaMA-B/L ImageNet-21K 224 ²	iLLaMA-B/L ImageNet-21K 224 ²
Fine-Tuning Configuration	ImageNet-1K	ImageNet-1K	ImageNet-1K
<i>Initialization:</i> weight init	trunc. normal (0.2)	trunc. normal (0.2)	trunc. normal (0.2)
<i>Training recipe:</i> optimizer optimizer momentum	AdamW $\beta_1, \beta_2=0.9, 0.999$	AdamW $\beta_1, \beta_2=0.9, 0.999$	AdamW $\beta_1, \beta_2=0.9, 0.999$
<i>Learning hyper-parameters:</i> base learning rate learning rate schedule weight decay batch size training epochs warmup schedule gradient clip exp. mov. avg. (EMA)	8e-5 cosine decay 1e-8 512 30 linear None None	8e-5/6e-5 cosine decay 1e-8 512 30 linear None None	1.1e-4/3.5e-5 cosine decay 1e-8 512 30 linear None None
<i>Dropout:</i> dropout rate stochastic depth rate	0.0 0.8	0.0 0.2/0.3	0.0 0.2/0.3
<i>Data augmentation:</i> input resolution randAugment random erasing label smoothing mixup cutmix	384 ² (9, 0.5) 0.25 0.1 0 0	224 ² (9, 0.5) 0.25 0.1 0 0	384 ² (9, 0.5) 0.25 0.1 0 0
<i>Soft mask:</i> soft mask schedule cutoff epochs lr warmup epochs	constant 0 0	constant 0 0	constant 0 0

Figure 1, but also outlines the training loss at each step. The general trend observed is that as the training loss of the models decreases, their accuracy increases.

Overall, the trend in changes for the base model is broadly similar to that of the tiny model. However, in contrast to the tiny model, the implementation of RoPE coupled with subsequent integration of LPE does not affect the base model’s performance. This lack of impact, we theorize, stems from the base regime’s reduced susceptibility to underfitting compared to the tiny regime, hence the addition of extra learnable parameters offers less benefit to its performance.

Notably, vanilla causal self-attention mechanism proves inadequate for model optimization, an issue effectively addressed by implementing the PS [CLS] method. Additionally, the application of the soft mask technique significantly contributes to the training efficacy of both model sizes.

D Rank Analysis of causal Self-attention

Detailed visualization results. We provide rank analysis results of all 3 heads in layer 1, 4, 8, 12 of ViT-T/16 and iLLaMA-T/16 in Figure 10. Besides the observation in Section 3.7, We make four observations: 1) Not each head in each layer of iLLaMA’s self-attention shows stronger concavity, suggesting that not every attention matrix of iLLaMA has a higher rank than its ViT counterpart. 2) In most cases, particularly in the shallow layers, the distribution of singular values in iLLaMA appears more uniform than in ViT. 3) In certain attention maps (e.g., layer 8, head 2, and layer 8,

Table 15: Our quantization-aware training settings for iLLaMa model on ImageNet-1K, adapted from [36, 33]. Some key training techniques are highlighted .

(Pre-)Training Configuration	iLLaMA-T/S ImageNet-1K
<i>Initialization:</i> weight init	trunc. normal (0.2)
<i>Training recipe:</i> optimizer optimizer momentum	AdamW $\beta_1, \beta_2=0.9, 0.999$
<i>Learning hyper-parameters:</i> base learning rate learning rate schedule weight decay batch size training epochs warmup schedule gradient clip exp. mov. avg. (EMA)	3e-3/4e-3 cosine decay 0.05 4096 300 linear None None
<i>Dropout:</i> dropout rate stochastic depth rate	0.0 0.0/0.1
<i>Data augmentation:</i> input resolution randAugment random erasing label smoothing mixup cutmix	224 ² (9, 0.5) 0.25 0.1 0.1/0.5 0.1/0.5
<i>Soft mask:</i> soft mask schedule cutoff epochs lr warmup epochs	constant/linear 50/50 5/5

Table 16: Our transfer learning settings for ViT-T and iLLaMa-T model on CIFAR10/100, respectively, adapted from [65]. Some key training techniques are highlighted .

Transfer Learning Configuration	CIFAR10	CIFAR100
<i>For both ViT-T and iLLaMA-T:</i> base learning rate batch size training epochs stochastic depth rate lr warmup epochs	2e-3 1024 300 0.0 50	2e-3 1024 300 0.0 50
<i>For iLLaMA-T only:</i> soft mask schedule cutoff epochs	linear 25	linear 50

head 3), the rank of ViT’s attention matrix is low, resulting in an skewed distribution of information. In contrast, such extreme cases were not observed in our iLLaMA. 4) The distribution of singular values in ViT varies significantly across different layers and heads (e.g., layer 1, head 1; layer 4, head 1; layer 8, head 1; layer 8, head 2), whereas iLLaMA’s distribution appears relatively more stable.

Table 17: ImageNet-1K classification accuracy via gradually replacing components in ViT-T/16 and ViT-B/16 with counterparts in LLaMA, **better** or **worse** than the ViT baseline results with our basic training recipe. Components from or modified from LLaMA are highlighted. P.E.: positional embedding, Bd.: bi-directional self-attention, Cs.: causal self-attention.

Ablation	FFN	Norm	Attention	P.E.	Tiny	Train Loss	Base	Train Loss
ViT [51]	MLP	LN	Bd.	LPE	72.2	-	81.8	-
results with our basic training recipe								
ViT	MLP	LN	Bd.	LPE	73.8	3.451	81.5	2.828
+ LLaMa FFN	SwiGLU	LN	Bd.	LPE	74.3	3.407	82.0	2.724
+ LLaMa Norm	SwiGLU	RMS	Bd.	LPE	74.5	3.406	81.7	2.721
+ LLaMa S.A.	SwiGLU	RMS	Cs.	LPE	0.1	Failed	0.1	Failed
+ LLaMa S.A.	SwiGLU	RMS	Cs. + <i>PS [CLS]</i>	LPE	71.9	3.599	80.6	2.869
+ LLaMa P.E.	SwiGLU	RMS	Cs. + <i>PS [CLS]</i>	RoPE	72.6	3.618	81.2	2.861
+ LPE P.E.	SwiGLU	RMS	Cs. + <i>PS [CLS]</i>	RoPE + LPE	73.2	3.531	81.2	2.839
modify the training techniques								
+ data aug.	SwiGLU	RMS	Cs. + <i>PS [CLS]</i>	RoPE + LPE	74.3	2.990	81.3	2.868
+ <i>soft mask</i>	SwiGLU	RMS	Cs. + <i>PS [CLS]</i>	RoPE + LPE	75.0	2.955	81.6	2.828

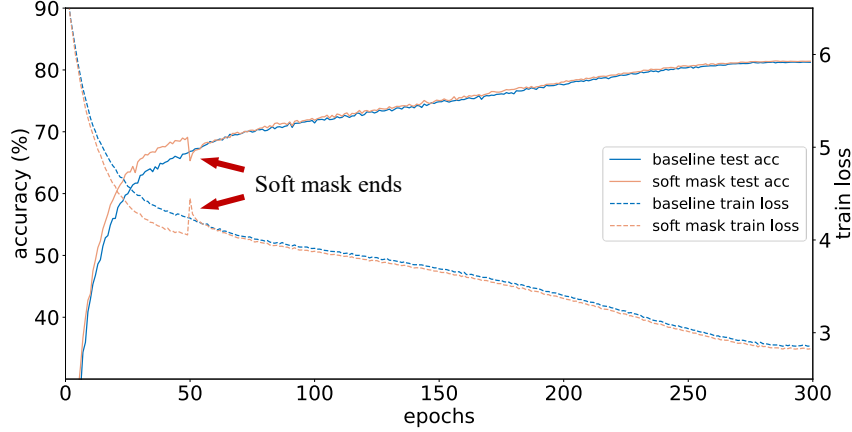


Figure 6: Training curves for iLLaMA-B/16 regime w/ and w/o soft mask. When soft mask ends, the model experiences a similar pattern to the training curve of iLLaMA-T/16 regime, with eventually a lower test loss observed.

E Analysis for Soft Mask Method

In this section, we plot the training results for iLLaMA-B/16 with and without the use of the soft mask technique in Figure 6. We can observe that the results display a similar pattern to those of iLLaMA-T/16 (Figure 3(b)).

We set the cutoff epochs to 50 and used a constant schedule. When the soft mask ends, there is a sudden increase in training loss and a steep decline in model accuracy. However, the final accuracy surpasses the baseline, and the training loss is also optimized to a lower value. Such phenomenon shows the versatility of the soft mask technique across models of varying capacities, and shows that causal self-attention can still effectively model even when a portion of the attention map is masked.

F Model Calibration

To qualitatively present the calibration property, we plot the reliability diagrams of ConvNeXt-B, DeiT3-B and the proposed iLLaMA-B using ImageNet-1K in Figure 7, following [59]. For well-calibrated models, the direction of accuracy in their reliability diagrams show a roughly diagonal pattern, *i.e.*, the difference between accuracy and confidence is small. Intuitively, the confidence

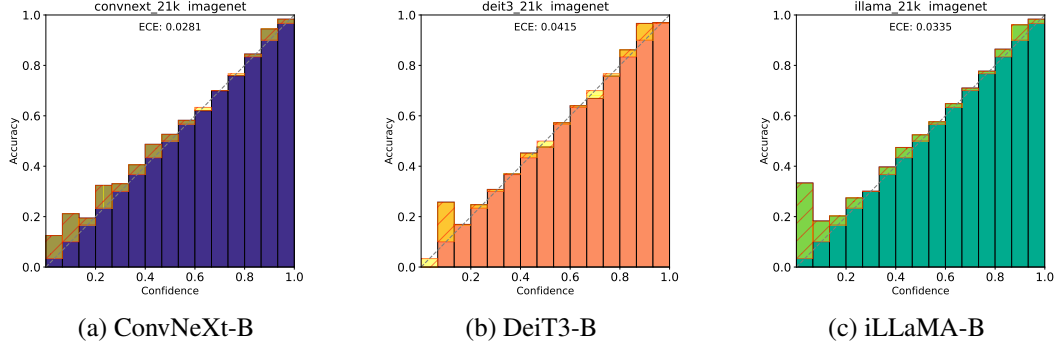


Figure 7: Calibration results of (a) ConvNeXt-B (b) DeiT3-B and (c) iLLaMA-B pretrained on ImageNet-21K and fine-tuned on ImageNet-1K.

of the early bins of the iLLaMA presents results below the accuracy level, indicating that iLLaMA tends to be underconfident. This observation, akin to that observed in the DeiT3, may be a common characteristic of Transformer-based architectures and was also noted in [59].

G Shape-Texture Bias

We visualize the shape-texture bias results on cue-conflict images of ConvNeXt-B, DeiT3-B and the proposed iLLaMA-B in Figure 8, following [59]. The three dashed lines of different colors represent the average shape decision of the three models over all categories. Generally, a more leftward average shape ratio indicates that the model relies more on global shape information for recognition tasks. iLLaMA shows higher shape scores relative to ConvNeXt and DeiT3.

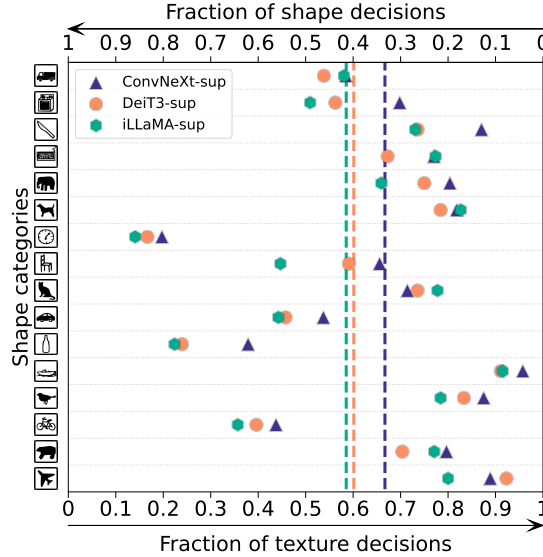


Figure 8: Shape-texture bias results of ConvNeXt-B, DeiT3-B and iLLaMA-B pre-trained on ImageNet-21K and fine-tuned on ImageNet-1K. sup: supervised learning paradigm.

H Loss Landscape

As shown in Figure 9, we visualized the loss landscape [32] of the iLLaMA-T/16 and ViT-T/16. The loss landscape of ViT and iLLaMA exhibits similar patterns, with the steepness and bumps observed in ViT seeming to be softened.

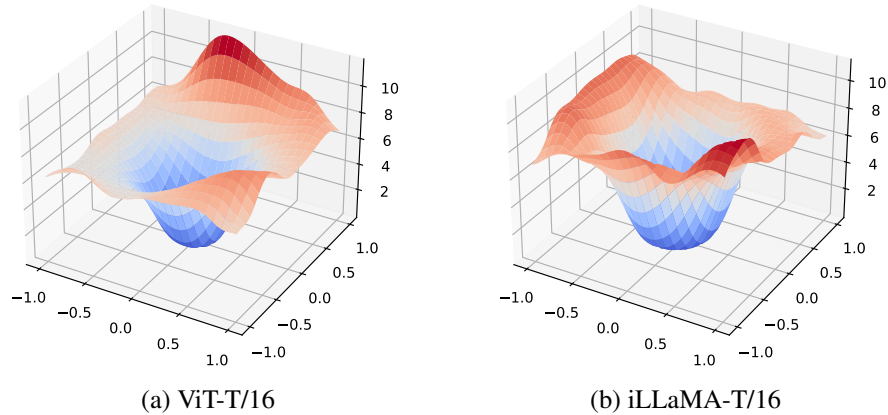


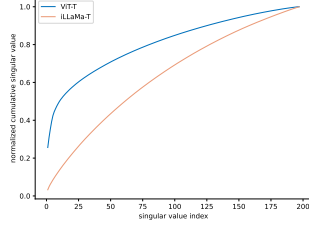
Figure 9: Loss landscape illustration of (a) ViT-T/16 and (b) iLLaMA-T/16.

I Limitations

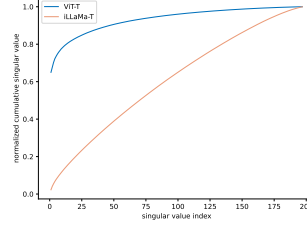
We have shown that the LLaMA architecture, enhanced by the developed post-sequence [cls] and soft mask techniques, is adept at adapting to tasks such as visual recognition and semantic segmentation. However, iLLaMA’s application remains predominantly within the realm of perception. In fact, such decoder-only architecture, favored by LLMs in the NLP field, can do more complex tasks, such as reasoning and generation. This may be due to their massive training data and the next sentence prediction training paradigm, which is not explored by iLLaMA. Thus, a critical validation step of aligning the architectures of text and visual models would be to construct a multi-modal large language model that fully leverages LLaMA components. In this envisioned model, both visual and textual feature extractors would be realized through the LLaMA architecture. Furthermore, we strongly argue that iLLaMA’s successful attempts at basic supervised training strategies and classification tasks provide a foundation for more complex tasks, such as object detection and depth estimation. This represents a compelling avenue for future research.

J Societal Impact

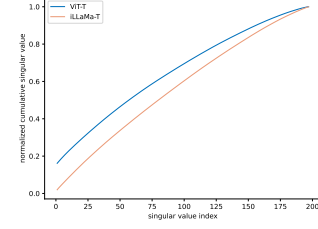
After the ChatGPT milestone in 2022, open-source architectures like LLaMA began to shine in the text domain. In the real world, images and text are the two main mediums of information and data types. For neural networks, having a unified architecture for language and vision models allows people to process these two distinct types of information using the same structure, which aids in the specialization of hardware implementation. This paper transfers the architecture widely used in language models to vision models, facilitating the achievement of this goal. The pretrained models and code provided in this paper can be used in a plug-and-play manner to serve this objective.



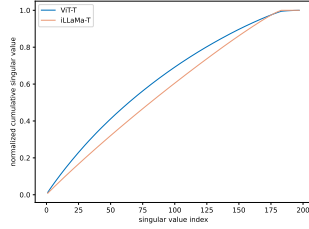
(a) layer 1, head 1



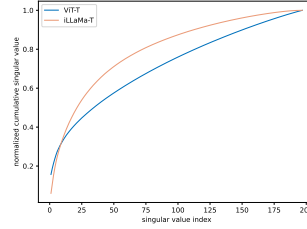
(b) layer 1, head 2



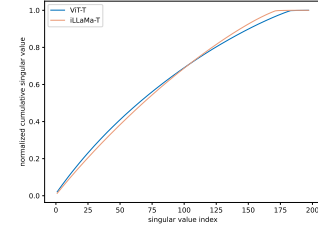
(c) layer 1, head 3



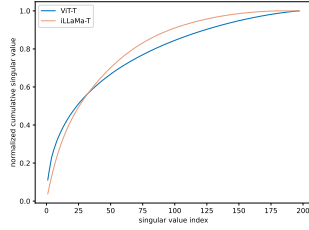
(d) layer 4, head 1



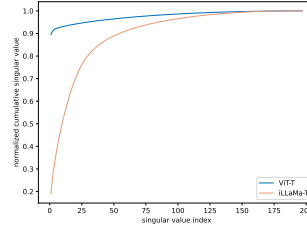
(e) layer 4, head 2



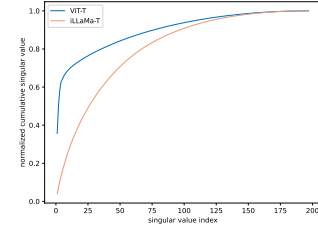
(f) layer 4, head 3



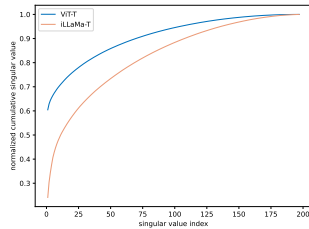
(g) layer 8, head 1



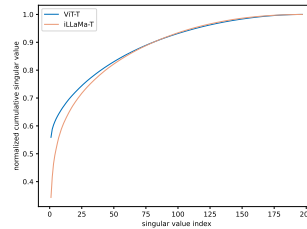
(h) layer 8, head 2



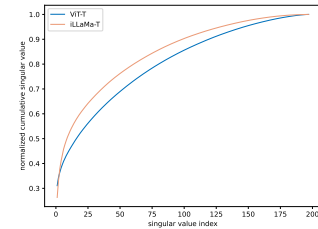
(i) layer 8, head 3



(j) layer 12, head 1



(k) layer 12, head 2



(l) layer 12, head 3

Figure 10: Rank analysis of the self-attention matrix of all 3 heads in layer 1, 4, 8, 12 of the pretrained ViT-T and iLLaMa-T with $N = 197$. In most cases, especially in shallow layers, the singular values of iLLaMa show a more uniform distribution than ViT.